Redox Biology 58 (2022) 102545

Contents lists available at ScienceDirect

Redox Biology

journal homepage: www.elsevier.com/locate/redox

Short-term hypoxia triggers ROS and SAFB mediated nuclear matrix and mRNA splicing remodeling

Chrysa Taze [a], Sotiria Drakouli [a], Martina Samiotaki [b], George Panayotou [b], George Simos [a,c], Eleni Georgatsou [a], Ilias Mylonis [a,*]

[a] Laboratory of Biochemistry, Faculty of Medicine, University of Thessaly, Biopolis, Larissa, 41500, Greece
[b] Institute for Bioinnovation, BSRC "Alexander Fleming", Vari, 16672, Greece
[c] Gerald Bronfman Department of Oncology, Faculty of Medicine, McGill University, Montreal, H4A 3T2, Canada

ARTICLE INFO

Keywords:
Hypoxia
Nuclear matrix
SAFB
Splicing
VEGFA

ABSTRACT

The cellular response to hypoxia, in addition to HIF-dependent transcriptional reprogramming, also involves less characterized transcription-independent processes, such as alternative splicing of the *VEGFA* transcript leading to the production of the proangiogenic VEGF form. We now show that this event depends on reorganization of the splicing machinery, triggered after short-term hypoxia by ROS production and intranuclear redistribution of the nucleoskeletal proteins SAFB1/2. Exposure to low oxygen causes fast dissociation of SAFB1/2 from the nuclear matrix, which is reversible, inhibited by antioxidant treatment, and also observed under normoxia when the mitochondrial electron transport chain is blocked. This is accompanied by altered interactions between SAFB1/2 and the splicing machinery, translocation of kinase SRPK1 to the cytoplasm, and dephosphorylation of RS-splicing factors. Depletion of SAFB1/2 under normoxia phenocopies the hypoxic and ROS-mediated switch in VEGF mRNA splicing. These data suggest that ROS-dependent remodeling of the nuclear architecture can promote production of splicing variants that facilitate adaptation to hypoxia.

1. Introduction

Oxygen deprivation (hypoxia) plays a critical role in both physiological and pathological conditions. It is often encountered inside solid tumors as a consequence of uncontrolled cell proliferation and aberrant vasculature [1]. Cells sense and respond to hypoxia primarily by extensive transcriptional reprogramming mediated by Hypoxia-Inducible Factors (HIFs). HIF activity relies on the stability of their oxygen-regulated HIF-α subunit. Their activation induces the expression of genes heavily involved in promoting cancer and resistance to therapy [2]. However, the early response to limited oxygen and, thus, transcription-independent events at the onset of hypoxia are poorly understood [3]. These include epigenetic marking of chromatin [4,5], changes in actin cytoskeleton [6], and alterations in mRNA processing and translation [7].

Much like hypoxia, alternative mRNA splicing is often linked to malignant phenotypes, being involved in proliferation, metastasis, and angiogenic signaling [8,9]. Effects of hypoxia on alternative splicing have been previously documented [10,11], albeit under conditions not excluding HIF-dependent transcriptional effects on the expression of splicing components and splicing variants. A prominent example of alternative mRNA splicing linked to oxygen levels is the processing of the *VEGFA* transcript leading to the generation of the pro-angiogenic form of the VEGF protein (VEGFa; [12]) in hypoxic cancer cells. mRNA splicing, both constitutive and alternative, involves the association of nascent mRNA transcripts with SR-protein splicing factors (often found deregulated in human cancers), which participate in both spliceosome assembly and splice site selection [13]. SR kinases such as SRPK1 govern this process by phosphorylating the RS-/SR-dipeptide motifs in splicing factors [14]. SR-protein hyperphosphorylation induces splicing factor assembly at nuclear speckles, while moderation of SR-phosphorylation levels is required for splicing and splice-site selection to proceed [14–16].

Notably, both SR-proteins and their modifying enzymes are reversibly bound to and regulated by components of the nuclear matrix, such as the family of the scaffold attachment factors B (SAFB) [14,17–19],

Abbreviations: HIF, Hypoxia-Inducible Factor; SAFB, Scaffold Attachment Factors B; SRPK1, Serine/Threonine-Protein Kinase SRPK1; VEGFA, Vascular Endothelial Growth Factor A; ROS, Reactive Oxygen Species; SF2, Arginine Rich Splicing Factor 1; DCFH-DA, 2′,7′-dichlorodihydrofluorescein diacetate.

* Corresponding author.
E-mail address: mylonis@med.uth.gr (I. Mylonis).

https://doi.org/10.1016/j.redox.2022.102545
Received 4 November 2022; Accepted 16 November 2022
Available online 17 November 2022

which participate in the functional organization of higher-order chromatin structures and proteins into domains and specific sites of control [18,20]. The SAFB family is composed of SAFB1, SAFB2, and SLTM (SAFB-like transcriptional modulator), highly similar proteins with roles in the regulation of transcription [21], response to stress, DNA damage [22,23] and control of the splicing machinery through direct associations with RNA, splicing factors or their modifying enzymes [14,18].

Here we describe an early transcription-independent mechanism, which, through ROS-dependent SAFB1/2 and splicing machinery nuclear redistribution, facilitates cancer cell response at the onset of hypoxia.

2. Materials and methods

2.1. Plasmids, cell culture, transfections and siRNA-mediated silencing

To construct Flag–HIF–1α the respective cDNA fragment was subcloned as *Bam*HI insert into pFLAG-CMV2 (Sigma-Aldrich, St Louis, MO, USA) vector after digesting with *Bam*HI the previously reported pEGFP–HIF–1α plasmid [24].

Human breast cancer MCF-7 cells (CVCL_0031; gifted from Dr. P. Moutsatsou originally acquired from ATCC) and human cervical carcinoma HeLa_S3 cells (CVCL_0058; ATCC), regularly tested for mycoplasma, were cultured in Dulbecco's modified Eagle's medium (DMEM; Biosera, Nuaille, France) supplemented with 10% FBS (Biosera Nuaille, France) and 100 U/mL penicillin–streptomycin (Biochrom, Berlin, Germany). Cells were routinely grown at 37 °C in an incubator with an adjusted humidified atmosphere composed of 95% air and 5% CO_2. For experiments under hypoxia, cells were incubated in an INVIVO2 200 hypoxia workstation (Baker Ruskinn, Sanford, ME) at 1% O_2 for the indicated time points. When needed, cells were treated with 1 mM DMOG, 1 μM actinomycin D, 1 mM NAC, 0.5 μM of rotenone or 100 μM H_2O_2 for the indicated time.

Transient transfections with plasmid DNA were carried out by using the JetPRIME® Polyplus reagent (Table 1) according to the manufacturer's instructions. For siRNA-mediated silencing, MCF-7 or HeLa cells were incubated in growth medium for 24 h with the indicated siRNAs in the presence of VIROMER®BLUE reagent (Table 1). Details on siRNA sequences are shown in Table 2.

2.2. Subcellular fractionation, SDS-PAGE and western blot

Three different fractionation methods were employed in order of simplicity (crude fractions) to the most elaborate (used for detailed analysis).

2.2.1. Crude fractionation

For soluble fractions, MCF-7 or HeLa cells were treated with (TNMT) lysis buffer (25 mM Tris pH 7.5, 150 mM NaCl, 1 mM $MgCl_2$, 1% w/v Triton-X100, 0.2 mM AEBSF. The soluble fraction was collected after centrifugation at 12000×*g* for 20min. Total fractions (TE) were collected by 2x Laemli Buffer and briefly sonicated at 60% amplitude (Vibra Cell, Sonics and Materials, USA).

Table 1
Kits and reagents used in this study.

Chemical/reagent	Reference
DMOG	400091, EMD Millipore, USA
Carboxy-H2DCFDA	C400, Invitrogen, USA
Rotenone	R8875, Sigma-Aldrich, Inc, USA
***N*-Acetyl-L-cysteine**	A9165, Sigma-Aldrich, Inc, USA
JetPRIME® Polyplus	Polyplus, Strasbourg, France
VIROMER®BLUE	Biontech, Germany
NucleoZOL	MACHEREY-NAGEL, Germany
High-Capacity Reverse Transcription kit	Applied Biosystems, Foster City, CA, USA
SYBR™ Select Master Mix	Applied Biosystems, Foster City, CA, USA

Table 2
List of non-target and specific siRNAs.

siRNA	Sequence (5′-3′)	Reference
AllStars Non target siRNA	Proprietary	1027280, Qiagen, USA
SAFB1 siRNA	CUGCCAUAUUGUAGCUCAAUA (dTdT)	Eurofins, France
SAFB2 siRNA	GAGUCAGGAUCGCAAGUCA(dTdT)	Eurofins, France
HIF-1α HP siRNA	AGGAAGAACTATGAACATAAA	SI02664053, Qiagen, USA
SF2/ASF siRNA(h)	Proprietary	sc-38319

2.2.2. Simple fractionation [24]

Cells were washed with cold PBS and treated with hypotonic buffer (15 mM KCl, 10 mM Hepes 7.4, 1.5 mM $MgCl_2$, 0.5 mM DTT, 0.1 mM AEBSF) and centrifuged (2000×*g*, 10min) to isolate the cytoplasmic proteins (CY) and a hypertonic buffer (10 mM MOPS 6.8, 250 mM $(NH_4)_2SO_4$, 3 mM $MgCl_2$, AEBSF) for the subsequent extraction of nuclear soluble proteins (nuclear soluble fraction; NS) after centrifugation at 10000×*g* for 15min. The remaining pellets were treated with 2%SDS and sonicated (Nuclear insoluble matrix fraction; NM).

2.2.3. Detailed fractionation (Fig. S1C)

Cells were washed with cold PBS and treated with hypotonic buffer A (15 mM KCl, 10 mM Hepes pH 7.5, 1.5 mM $MgCl_2$, 0.5 mM DTT, 0.1 mM AEBSF) and centrifuged (5000×*g*, 10min). Pellet (crude nuclei) was purified by using a "sucrose cushion" (Sucrose 1.5 M, 25 mM KCl, 50 mM Hepes pH 7.5, 5 mM $MgCl_2$, 0.5 mM DTT, 0.1 mM AEBSF) and centrifuged (10000×*g*, 45min). To acquire the nucleoplasmic fraction (NP) purified nuclei were treated with buffer B (10 mM Hepes pH 7.5, 150 mM NaCl, 300 mM sucrose, 3 mM $MgCl_2$, 0.5% Triton X-100, 0.5 mM DTT, 0.1 mM PMSF) and centrifuged for 15min at 10000×*g*. Pellets were washed, resuspended in buffer B, and incubated at 32 °C for 10min with RNAse (0.4 μg; Macherey-Nagel, Duren, Germany) and then centrifuged at 10000×*g* for 10min in order to receive the RNA-rich fraction (RN). The remaining pellets were resuspended in buffer B and incubated at 37 °C for 10min with DNAse (0.5 μg; Promega, Madison, WI, USA) and centrifuged at 10000×*g* for 10min in order to receive the DNAse-treated fraction (DN). Finally, to receive the insoluble nuclear matrix fraction (NM), pellets were treated with 2 M NaCl in 2%SDS and sonicated (Vibra Cell, Sonics and Materials, USA).

2.2.4. Total extracts

To obtain total cellular extracts cells were 2xLaemli Buffer (65 mM Tris-Cl 6.8, 2% SDS, 10% glycerol, 0.05% Bromophenol Blue, 25 mM DTT), boiled and sonicated at 60% amplitude (Vibra Cell, Sonics and Materials, USA).

2.3. Western blotting

Samples were adjusted and loaded for SDS/PAGE electrophoresis as equal number of cells in each lane. Protein samples were resolved by 10% SDS/PAGE and analyzed by western blotting using specific antibodies (Table 3). Western blotting images were taken using an Uvitec Cambridge Chemiluminescence Imaging System (Uvitec Cambridge, Cambridge, UK) using Alliance software, version 16.06 and quantified by Uviband Software (Uvitec Cambridge, Cambridge, UK).

2.4. Immunoprecipitation and mass spectrometry analysis

2.4.1. Immunoprecipitation

To immunoprecipitate nuclear (both soluble and matrix associated) SAFB1 or SAFB2 and assess their binding with other proteins, MCF-7 cell

Table 3
Primary and secondary antibodies used in the study.

Primary Antibodies		
Antibody	Reference	Working dilution
Rabbit polyclonal anti-SAFB1 (specific)	A300-811A, Bethyl laboratories, Inc, USA	WB and IF 1:1000 IP 1 μg per 1 mg protein
Rabbit polyclonal anti-SAFB2 (specific)	A301-112A, Bethyl laboratories, Inc, USA	WB and IF 1:2000 IP 1 μg per 1 mg protein
Mouse monoclonal anti-SAFB (SAFB1/2 common)	SAB2702149,Sigma-Aldrich, Inc, USA	WB and IF 1:1000 IP 1 μg per 1 mg protein
Mouse monoclonal anti-SRPK1	611072, BD Transduction Laboratories	WB and IF 1:1000
Mouse monoclonal anti-Lamin B1	sc-374015, Santa Cruz Biotechnology, Inc USA	WB 1:500 IF 1:1000
Mouse monoclonal anti-SF2	sc-33652 Santa Cruz Biotechnology, Inc USA	WB and IF 1:500 IP 1 μg per 1 mg protein
Rabbit polyclonal anti-Hsp70	SPA-812 StressGen Enzo Life Sciences, USA	WB 1:1000
Mouse mab104	[37]	WB 1:2000
Mouse monoclonal anti- β-Actin	3700S, Cell Signaling, USA	WB 1:5000
Mouse monoclonal anti- α -tubulin	3873S, Cell Signaling, USA	WB 1:10000
Rabbit anti-HIF-1α	[62]	WB 1:1000
Secondary antibodies		
Antibody	Reference	Working dilution
Goat Anti-Rabbit HRP	AP187P, EMD Millipore, USA	WB 1:5000
Horse Anti-Mouse HRP	7076, Cell Signaling, USA	WB 1:3000
Anti-rabbit IgG Fab2 488	4412S, Cell Signaling, USA	IF 1:500
Cy™3-Goat Anti-Mouse IgG (H + L) Conjugate	81-6515, Invitrogen, USA	IF 1:500

nuclei were lysed in a buffer containing 200 mM NaCl, 25 mM Hepes pH 7.4, 2 mM $MgCl_2$, 1% Triton, 0.1 mM AEBSF and DTT. The corresponding antibodies (1 μg) were added to the lysates (~1.5 mg total protein) and the mix was incubated for 2 h at 4 °C. The mix was then added to prewashed protein A beads (Santa Cruz Biotechnology) and the incubation continued under rotation for 16 h at 4 °C. After three consecutive washes with the extraction buffer the immuno-precipitates were eluted by adding glycine buffer (0.2 M glycine pH 2.2, 0.5 M NaCl) to the beads. Eluates were equilibrated with Tris-HCl pH 8.5 and the samples were further processed either by FASP mediated tryptic digestion and analyzed by mass spectrometry or analyzed by western blotting with corresponding antibodies (Table 3).

2.4.2. Mass spectrometry

Ultra-high pressure nanoLC: 2.5 μg peptides were pre-concentrated with a flow of 3 μL/min for 10 min using a C18 trap column (Acclaim PepMap100, 100 μm × 2 cm, Thermo Fisher Scientific, Waltham, MA, USA) and then loaded onto a 50 cm long C18 column (75 μm ID, particle size 2 μm, 100 Å, Acclaim PepMap100 RSLC, Thermo Scientific). The binary pumps of the HPLC (RSLCnano, Thermo Fisher Scientific, Waltham, MA, USA) consisted of Solution A (2% (v/v) ACN in 0.1% (v/v) formic acid) and Solution B (80% (v/v) ACN in 0.1% (v/v) formic acid). The peptides were separated using a linear gradient of 4% B up to 40% B in 230 min with a flow rate of 300 nL/min. The column was placed in an oven at 60 °C.

LC-MS/MS: Eluted peptides were ionized by a nanospray source and detected by an LTQ Orbitrap XL mass spectrometer (Thermo Fisher Scientific, Waltham, MA, USA) operating in a data dependent mode (DDA). Full scan MS spectra were acquired in the orbitrap (m/z 300–1600) in profile mode with resolution set to 60,000 at m/z 400 and automatic gain control target at 106 ions. The six most intense ions were sequentially isolated for collision-induced (CID) MS/MS fragmentation and detection in the linear ion trap. Dynamic exclusion was set to 1 min and activated for 90 s. Ions with single charge states were excluded. Lockmass of m/z 445,120025 was used for continuous internal calibration. XCalibur (Thermo Fisher Scientific, Waltham, MA, USA) was used to control the system and acquire the raw files. Protein identification and quantification. The raw mass spectral files were processed using MaxQuant software (version 1.6.3.3; https://maxquant.net/maxquant/) with default parameters for protein identification and quantification. Trypsin specificity was set to allow two missed cleavages and minimum peptide length was set to 7 amino acids. Cysteine carbamidomethylation was set as fixed, and methionine oxidation, serine-threonine-, tyrosine-phosphorylation, deamidation of asparagine and glutamine and N-terminal acetylation were set as variable modifications. A maximum of 5 modifications per peptide was set. The false discovery rate both for peptide and protein was set to 1%. For calculation of protein abundances, label-free quantification (LFQ) was performed with both "second peptides" and "match between run" options enabled. The human FASTA files were from UniProt downloaded on June 28, 2018. To determine methionine oxidation status under hypoxia or normoxia by mass spectrometry the data for methionine-sulfoxide-containing (Met-SO) peptides were converted to a fraction of oxidized vs the non-modified peptides in each condition (Ratio mod/base; Table S1) and a score with a threshold of more than 100 was set to increase confidence (Table S1).

Proteomic data analysis: Statistical analysis was performed using Perseus (1.6.15.0; https://maxquant.net/perseus/) [25]. Proteins identified as contaminants, "reverse" and "only identified by site" were filtered out. Additionally, the identified proteins were assessed for their presence in the CRAPome database (v.2.0 https://reprint-apms.org/?q=chooseworkflow) [26]. The LFQ intensities were transformed to logarithmic values [log2(x)]. The label-free quantified proteins were subjected to statistical analysis with Student t-test (permutation-based FDR-value with 0.05 cutoff). LC-MS/MS data after statistical analysis were plotted in a volcano graph based on the difference between the two samples expressed as log2(x) versus their statistical significance expressed as –Log10(p-value). Hierarchical clustering was carried out on Z-score transformed LFQ values using average linkage using Euclidean distance.

SAFB1 and SAFB2 interacting proteins' lists were compared by Venny 2.1 [27]. Gene Ontology, Biological Process (BP), or Molecular Function (MF) were performed with ShinyGO 0.76 [28]. Physical and functional association networks were performed with STRING 11.5 [29].

2.5. RNA extraction and quantitative RT-PCR

Total RNA isolation was performed by using the NucleoZOL reagent (Table 1) and cDNAs were synthesized by the High-Capacity Reverse Transcription kit (Table 1). Quantitative PCR was carried out in a LightCycler® 96 System (Roche, Basel, Switzerland), using the SYBR Select master mix (Table 1). The mRNAs encoding for VEGFtotal, VEGFa isoform, VEGFb isoform, LDHA total, LDHA-001, BNIP3 total, BNIP3Δex2 and ACTIN were amplified using primers shown in Table 4. Each sample was assayed in triplicate for all targets and internal control. Relative quantitative gene expression was calculated using the ΔΔCT method and presented as a fold change in relation to total VEGF, LDHA and BNIP3 in normoxia.

2.6. Immunofluorescence

Immunofluorescence microscopy experiments were performed as previously described [17]. In brief, cells were grown on coverslips and

Table 4
Primers for RT-PCR

Primer designation	Sequence (5′-3′)
VEGFa variants	F 5′ TCCCTGTGGGCCTTGCTC 3‘
	R 5’ GCCTCGGCTTGTCACAT 3‘
VEGFb variants	F 5’ TCCCTGTGGGCCTTGCTC 3‘
	R 5‘ GATCTGGTTCCCGAAACCC 3‘
VEGF Total	F 5‘ CCCACTGAGGAGTCCAACATC 3‘
	R 5‘ GGCCTTGGTGAGGTTTGATC 3‘
ACTIN	F 5’ CCAACCGCGAGAAGATGA 3′
	R 5′ CCAGAGGCGTACAGGGATAG 3′
LDHA-001	F 5′ CGGATCTCATTGCCACGC 3′
	R 5′ AGCTGATCCTTTAGAGTTGCCA 3′
LDHA total	F 5′ GGATCTCCAACATGGCAGCCTT 3′
	R 5′ AGACGGCTTTCTCCCTCTTGCT 3′
BNIP3Δex2	F 5′ ATGTCGCAGAACGGAGCGC 3′
	R 5′ TCAAGATGCTTTCAACTTCTTTCC 3′
BNIP3 total	F 5′ TCAGCATGAGGAACACGAGCGT 3′
	R 5′ GAGGTTGTCAGACGCCTTCCAA 3′

fixed with 3,7% formaldehyde in PBS for 10 min, permeabilized with 0.1% Triton-X 100 at 4 °C for 15 min, and treated with 1% BSA in PBS for 1 h at room temperature. Then, coverslips were incubated overnight at 4 °C with specific antibodies (Table 3), washed twice with PBS, and incubated for 1 h at room temperature with appropriate secondary antibodies (Table 3). Cells were counterstained with DAPI (4′,6-diamidine-2′-phenylindole dihydrochloride; Sigma Aldrich, St Louis, MO, USA), mounted on slides, and visualized.

In order to observe the nuclear matrix-bounded SAFB1/2 after a pre-extraction step cells were pre-treated with a buffer containing 10 mM Pipes pH 6.8, 100 mM NaCl, 300 mM sucrose, 3 mM $MgCl_2$, 1 mM EGTA, 0.5% Triton-X100, for 5min. Then cells were washed with PBS, fixed with 4%PFA for 10min and blocked with 1% BSA as above.

For SRPK1 fluorescence staining, cell fixation was performed with 100% methanol for 8min at −20 °C and then treated and observed as above.

All images were visualized with a Zeiss Axio Imager.Z2 microscope equipped with AxioCam MRm sensor and a 40 × /0.75 objective or a 100 × /1.3 oil-immersion lens through Zeiss Immersol 518 F. Zeiss filter sets included Fs02 (G365/FT510/LP420), Fs09/AF488 (BP450-490/FT510/LP515), and Fs14/AF546 (BP510-560/FT580/LP590), images were collected by using Zeiss Zen 2011 (blue edition, ver. 1.0.1.0) image acquisition software. For quantification, cells were captured with the same exposure time at 22 °C (room temperature). Images were saved at 880 × 684 pixels (90.10 × 70.03 μm) in tagged image file format for downstream analysis. Image quantification was done on unmodified images, data were compared by Student's two-tailed *t*-test and represented as means ± SEM. For representation purposes, images were enhanced, split, or cut using imageJ (NIH, Bethesda, MD, USA) to accurately reflect actual relationships between factors that were quantified from unmodified images.

2.7. Image analysis

All collected images were processed with imageJ (NIH, Bethesda, MD, USA). Collected microscopy images shown in the figures were deconvolved using the PSF-based Iterative Deconvolve 3D deconvolution plugin for imageJ with default plugin settings and 2 iterations. To estimate the number of SAFB1 or SAFB2 accumulated-foci images were equally thresholded and analyzed by the *Analyze Particles* plugin provided with imageJ and the number of foci counts/cell, total foci area/cell and average size of foci were determined. Quantitation of the fluorescence was performed by using ImageJ and expressed as fluorescence intensity. It involved outlining each cell area and measurement of area, fluorescence intensity and adjacent background. Calculating total corrected cellular fluorescence (for cytoplasmic or nuclear signal) = integrated density – (selected area × mean fluorescence of background) [30].

2.8. Detection and quantification of ROS using DCFH-DA

To detect the ROS production cells were cultured on coverslips or in 96 well plates and incubated with 5 μM (final concentration) DCFH-DA diluted in PBS for 30min at 37 °C. Then PBS was removed, DMEM was added, and cells were cultured in normoxia or hypoxia for 15min to 4 h. ROS production was either observed with a Zeiss Axio Imager.Z2 microscope equipped with AxioCam MRm sensor, using the green channel or their fluorescence intensity was quantified by using the Spark® multimode microplate reader (Tecan Trading AG, Switzerland).

2.9. Statistical analysis

Statistical differences between two groups of data were evaluated by using the GraphPad Prism version 5.04 software. Differences were tested by Student's t-test (two-tailed) between two groups or by one-way analysis of variance (ANOVA) within multiple groups; $P < 0.05$ was deemed statistically significant.

3. Results

3.1. *Short-term hypoxia promotes the production of a pro-angiogenic VEGFA splicing variant concomitantly with intranuclear redistribution of SAFB1/2 and their dissociation from the nuclear matrix*

To explore the effect of short-term hypoxia on splicing, we focused on the expression of *VEGFA* mRNA (a prominent example of alternative splicing in cancer) and its alternatively spliced forms (VEGFa and VEGFb) in MCF7 cells after 2 h incubation at normoxia (21% O_2) or hypoxia (1% O_2) (Fig. 1A; left panel). Although 2 h-exposure to hypoxia slightly increased but did not significantly change total *VEGFA* mRNA levels (Fig. 1A; graph in magenta), the balance between the anti-angiogenic VEGFb and pro-angiogenic VEGFa forms was significantly shifted towards the pro-angiogenic splicing variant under hypoxia (Fig. 1A; right graph). In support of this observation, the expression of two other well-characterized HIF target genes *BNIP3* and *LDHA* (Fig. S1A left panel), under the same conditions, showed that short-term hypoxia significantly affected the expression of their splicing variants BNIP3ΔEx2 (skipping exon 2; [31]) and LDHA-001 (alternative exon1; [10]) without affecting their total expression level to a significant degree (Fig. S1A right graphs). To investigate the mechanism that underlies this early effect of hypoxia on splicing, we first examined the SAFB proteins, previously shown to associate with splicing machinery components [17,19,32]. Brief (2-h) exposure of cells to hypoxia caused significant disassembly of the SAFB1/2 intranuclear foci (corresponding to their typical nuclear matrix location), suggesting their dispersal in the nucleoplasm (Fig. 1B). These results were even more apparent when pre-extraction of soluble proteins was performed before cell fixation in the immunofluorescence microscopy experiments in order to avoid background noise of the fluorescent signal (Figs. S1B and C). In support of these observations, detailed biochemical fractionation (Fig. S1D) of the same cells demonstrated the significant relocation of SAFB1/2 from the insoluble nuclear matrix fraction (NM) and their recovery in a soluble nuclear fraction rich in RNA and RNA-associating proteins (RN) (Fig. 1C and D).

3.2. *Hypoxic dissociation of SAFB1/2 from the nuclear matrix is fast, HIF-independent, and reversible upon reoxygenation*

A detailed time course of the hypoxic dissociation of SAFB1/2 from the nuclear matrix, by monitoring SAFB1/2 levels in total protein extracts and a fraction containing only soluble proteins of MCF7 cells revealed that, although total SAFB1/2 levels were not affected by

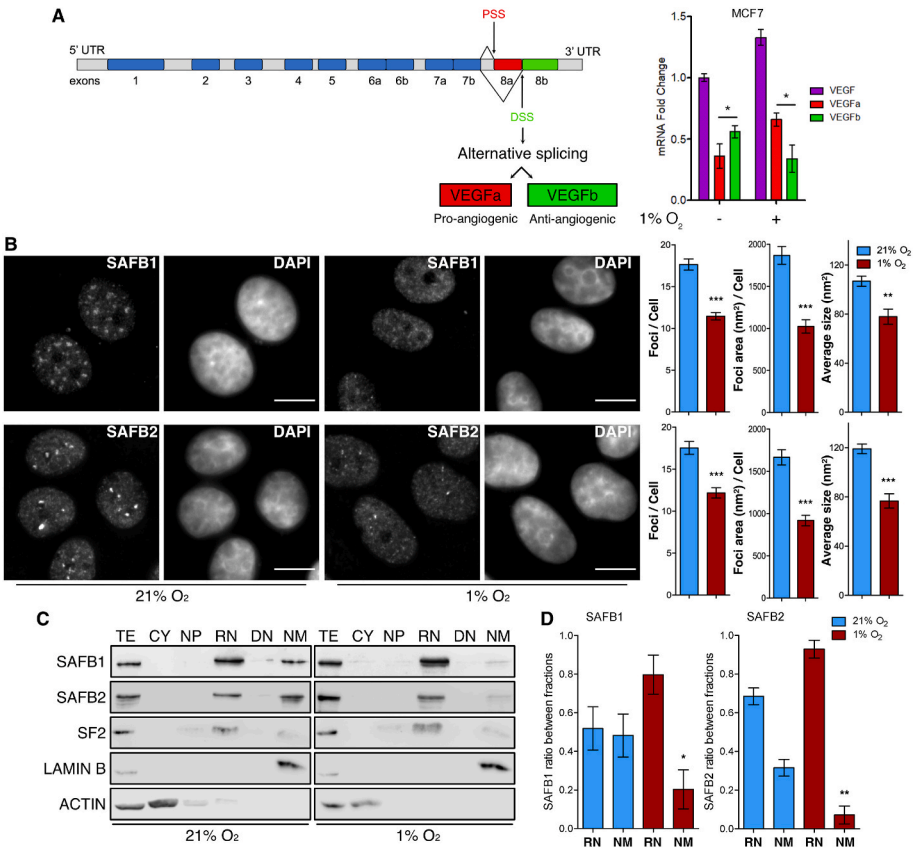

Fig. 1. Short term hypoxia effects on VEGF mRNA splicing are concomitant with intranuclear redistribution of SAFB1/2 and its dissociation from the nuclear matrix.

A Schematic representation of *VEGFA* (left panel) indicating the alternatively spliced forms of exon 8 resulting in the production of pro-angiogenic VEGFa (red) or anti-angiogenic VEGFb form (green). Arrows show Proximal Splice Site (PSS; red) and Distal Splice Site (DSS; green) selected by the splicing machinery to produce the indicated spliced forms. mRNA fold change levels (right panel) of total *VEGFA* (magenta) or its alternatively spliced forms (VEGFa: red; VEGFb: green) were determined by RT-PCR in MCF-7 cells incubated at 21% or 1% O_2 for 2 h. Results are shown as ratios in relation to the total *VEGFA* levels in normoxia and represent the mean of three independent experiments performed in triplicates ± s.d. (n = 9; $*P < 0.05$).

B Immunofluorescence microscopy images (left panels) of MCF7 cells grown on coverslips at 21% or 1% O_2 for 2 h using antibodies against SAFB1 or SAFB2 (As indicated). Nuclei were stained with DAPI (Scale bars: 10 μM). Graphs (right panels) represent the quantification of SAFB1 (upper panels) or SAFB2 (lower panels) foci/cell, their total area/cell and average size from a total of 80–100 individual cells from two independent experiments in each condition ±s.e.m. ($***P < 0.001$; $**P < 0.01$).

C Immunoblotting analysis of subcellular fractions (TE: Total Extracts, CY: Cytoplasmic fraction, NP: Soluble nucleoplasmic fraction, RN: Soluble nuclear fraction after RNase treatment, DN: Soluble nuclear fraction after DNase treatment, NM: Nuclear Matrix fraction; see also Fig.ure S1C) of MCF-7 cells incubated at 21% or 1% O_2 for 2 h (as indicated) using antibodies against the indicated proteins. SF2, Lamin B, and actin were used as fractionation controls for RNAse treated, nuclear matrix and cytoplasmic fraction respectively.

D Quantitative analysis of immunoblots (shown in C) depicting the SAFB1 or SAFB2 ratio (as indicated) between RT (RNase treated) and NM (Nuclear Matrix) fractions after the indicated treatment. Columns represent the mean of three independent experiments ±s.e.m. (n = 3; $*P < 0.05$, $**P < 0.01$).

hypoxia, increased recovery of SAFB1/2 in the soluble fraction occurred very early (15 min) after the onset of hypoxia (Fig. 2A). Same results were also obtained using HeLa cell extracts (Fig. S1E). Moreover, this swift hypoxic SAFB1/2 solubilization was quickly reversed upon reoxygenation (Fig. 2B). Since the cellular response to hypoxia is predominantly mediated by changes in the activity of HIF hydroxylases, their implication in SAFB1/2 removal from the nuclear matrix under hypoxia was then examined using DMOG (an established prolyl-hydroxylase (PHD) inhibitor). Treatment of MCF7 cells with DMOG induced, as expected, the expression of HIF-1α levels, but, unlike hypoxia, it did not affect SAFB1/2 solubilization (compare Fig. 2C and A). Moreover, as PHD inactivation ultimately affects the transcriptional activity of HIF, HIF-1α was overexpressed or depleted. Overexpression of Flag–HIF–1α under normoxia or HIF-1α depletion under hypoxia in MCF7 cells was also without effect on SAFB1/2 recovery in the soluble fraction (Fig. 2D and E, respectively). HIF-1α depletion in a HeLa cell strain not expressing HIF-2α [33] confirmed that neither HIF-1 nor HIF-2 activity is implicated in SAFB1/2 redistribution (Fig. S1F). Furthermore, analysis of the expression of *VEGFA* mRNA variants in the same HIF-1α-depleted HeLa cells showed that reprogramming of *VEGFA* splicing at early hypoxia is HIF-independent (Fig. S1G). Finally, hypoxia-inducible SAFB1/2 redistribution was not affected in MCF7 cells treated with actinomycin D, excluding the involvement of the general transcription machinery (Fig. 2F). Overall, our data strongly suggest that the reversible dissociation of SAFB1/2 from the nuclear matrix and its subsequent intranuclear redistribution caused by short-term hypoxia is independent of HIF-hydroxylation and HIF-regulated transcription.

3.3. *Disassembly of intranuclear foci and solubilization of SAFB1/2 under hypoxia are ROS-dependent*

An early, time-dependent, effect of oxygen deprivation on cultured cells is the increased production of reactive oxygen species (ROS) due to mitochondrial dysfunction [34–36]. ROS production (measured by DCFH-DA fluorescence) was indeed observed inside our MCF7 cells upon their incubation under hypoxia, being detected after 30 min and reaching a peak at around 2 h after the onset of hypoxia (Fig. 3A and S2A). Neutralization of ROS by the antioxidant n-acetyl cysteine (NAC; Fig. 3A) reversed the hypoxic dissociation of both SAFBs from their distinct intranuclear foci and restored their foci distribution both in terms of number and average size (Fig. 3B). Additionally, biochemical fractionation confirmed that NAC restored the association of SAFB with the nuclear matrix fraction under hypoxic conditions (Fig. S2B). To demonstrate the role of ROS in a positive way, the respiratory chain inhibitor rotenone was used in the place of hypoxia to induce mitochondrial ROS production (Fig. 3C). Treatment with rotenone indeed phenocopied the hypoxic disassembly of the SAFB1/2 intranuclear foci and their redistribution in a more diffuse pattern inside the nucleus (Fig. 3D). Furthermore, analysis of fractions derived from MCF7 cells after a brief treatment with either rotenone or H_2O_2 revealed a significant SAFB redistribution in soluble nuclear fractions (Fig. 3E and Fig. S2C respectively), confirming that the dissociation of SAFB1/2 from

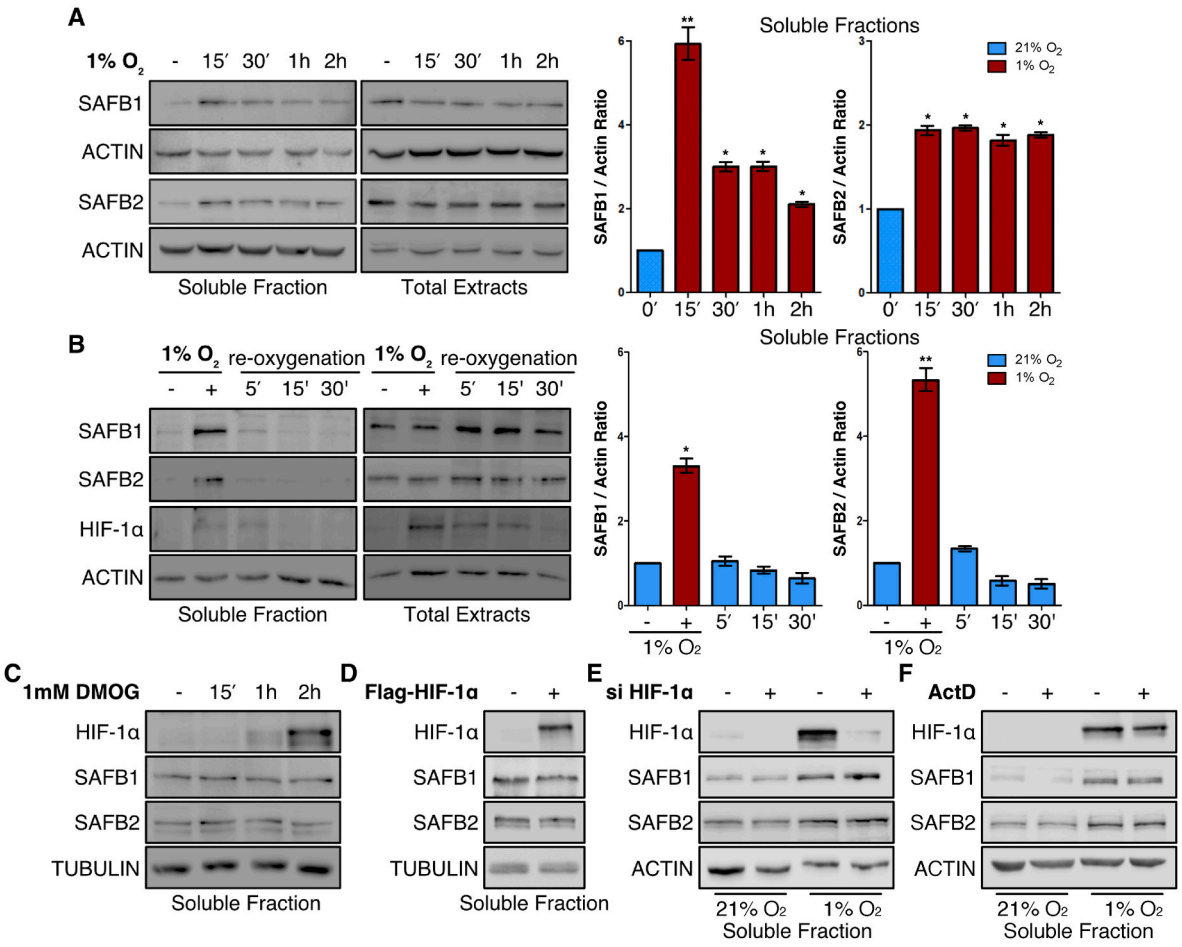

Fig. 2. Hypoxic dissociation of SAFB1/2 from the nuclear matrix is fast, HIF-independent and reversible upon reoxygenation.
A Western blot analysis of proteins recovered in a soluble fraction (left panels) and a total cell extract (right panels) of MCF7 cells incubated under 1% O_2 for the indicated time. Graphs represent the quantitative analysis of immunoblots (soluble fractions) depicting the SAFB1 or SAFB2 ratio over actin (as indicated) after the indicated treatment. Columns represent the mean of three independent experiments ±s.e.m. (n = 3; *P < 0.05, **P < 0.01).
B Western blot analysis of proteins recovered in a soluble fraction (left panels) and a total cell (right panels) of MCF7 cells incubated under 1% O_2 for 2 h followed by re-oxygenation for the indicated time. Graphs represent the quantitative analysis of immunoblots (soluble fractions) depicting the SAFB1 or SAFB2 ratio over actin (as indicated) after the indicated treatment. Columns represent the mean of two independent experiments ±s.e.m. (n = 2; *P < 0.05, **P < 0.01).
C Immunoblotting of soluble proteins of MCF7 cells incubated with 1 mM DMOG for the indicated time.
D Immunoblotting of soluble proteins of MCF7 cells overexpressing Flag–HIF–1α under normoxia.
E Western blotting of soluble proteins of MCF7 cells incubated at 21% or 1% O_2 for 2 h after silencing HIF-1α expression by siRNA (as indicated).
F Western blotting of soluble proteins of MCF7 cells incubated at 21% or 1% O_2 for 2 h with or without 1 μM actinomycin D (as indicated).
Images are representative of two (B–F) or three (A) independent experiments.

the nuclear matrix is triggered by ROS production under short-term hypoxia.

3.4. Short-term hypoxia abolishes the association of SAFB1/2 with essential components of splicing machinery and chromatin organization

To investigate further the possible link between the dissociation of SAFB1/2 from the nuclear matrix and the reprogramming of VEGF mRNA splicing observed under the same short-term hypoxic conditions, we analyzed the SAFB1/2 interactome under normoxia or hypoxia. Proteomic analysis on SAFB1/2 immunoprecipitates from total nuclear fractions (containing both soluble and nuclear matrix-associated proteins) extracted from MCF7 cells using high salt and detergent concentration, showed that short-term hypoxia significantly affected the interactome landscape of SAFB1/2. Out of the 150 total precipitated proteins (Fig. S3A; Table S1), 56 proteins exhibited altered SAFB1/2 association when compared to normoxic conditions (Fig. 4A; Volcano plots comparing the normoxic versus the hypoxic SAFB1 and SAFB2 interactomes ($p < 0.05$)). GO biological process enrichment and protein-protein interaction analysis and clustering (STRING analysis) of these 56 proteins showed that they are mainly implicated in mRNA processing and regulation of gene expression (Figs. S3B and S4A). Out of these, only a minority (7 proteins with RNA and lipid binding abilities) exhibited increased association with either SAFB1 or SAFB2 under hypoxia (Fig. 4A, green-colored dots; Fig. S4B; Table S1), while the majority (49 proteins) lost their association with SAFB1 or SAFB2 under hypoxia (Fig. 4A, red-colored dots; Table S1). Proteins that lost their interaction with either SAFB1 or SAFB2 under hypoxia (Fig. 4B) were proteins involved in RNA processing (Fig. 4C–E; Figs. S5A and C). The group of specific SAFB1 and SAFB2 normoxic interactors also contained proteins involved in the regulation of gene expression and conformation of DNA, respectively (Fig. 4C and D and Figs. S5A and B). Common SAFB1 and SAFB2 interactors (16 proteins in total; Fig. 4E) were mainly implicated in RNA processing, splicing, and DNA conformation (Fig. 4E and Fig. S5C). These results strongly suggest that short-term hypoxia affects the physical interactions between SAFB1/2 and components of the mRNA processing and splicing machinery, including members of the SR-family of splicing factors as well SRPK1, the kinase that phosphorylates

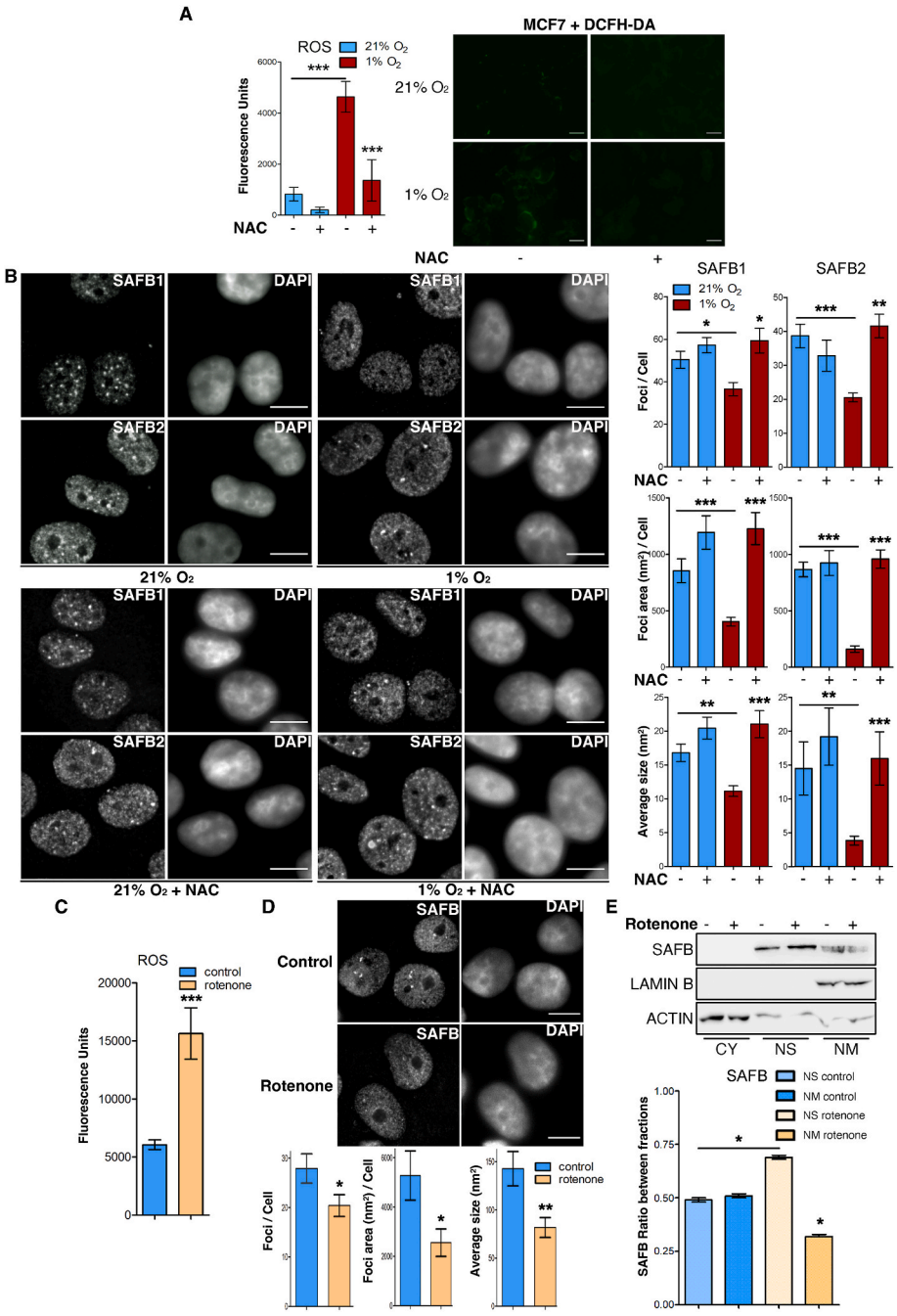

Fig. 3. Disassembly of intranuclear foci and solubilization of SAFB1/2 under hypoxia are ROS-dependent.

A ROS production in MCF7 cells incubated at 21% or 1% O_2 for 2 h without or with 1 mM *N*-acetyl-cysteine (NAC; as indicated). Left panel: DCFH-DA fluorescence units. Values are the mean of three independent experiments performed in triplicates ± s.d. (n = 9; ***$P < 0.001$). Right panel: Representative fluorescent microscopy images showing the DCFH-DA signal.

B Immunofluorescence microscopy images (left panels) of MCF7 cells grown under 21% or 1% O_2 for 2 h using antibodies against SAFB1 or SAFB2 and treated or not with 1 mM NAC (as indicated). Nuclei were stained with DAPI (Scale bars: 10 μM). Graphs (right panels) show quantification of SAFB1 or SAFB2 foci number/cell, total area/cell and average size (as indicated) from a total of 90–110 individual cells from two independent experiments in each condition ±s.e.m. (***$P < 0.001$; **$P < 0.01$; *$P < 0.05$).

C ROS production is shown as DCFH-DA fluorescence units in MCF7 cells treated without or with rotenone (as indicated). Values are the mean of three independent experiments performed in triplicates ± s.d. (n = 9; ***$P < 0.001$).

D Immunofluorescence microscopy images (upper panels) of MCF7 cells using antibodies against SAFB1/2 and treated or not with 0.5 μM of rotenone for 30 min (as indicated). Nuclei were stained with DAPI (Scale bars: 10 μM). Graphs (bottom panels) represent the quantification of SAFB1/2 foci number/cell, total area/cell and average size (as indicated) from a total of 70–80 individual cells from two independent experiments in each condition ±s.e.m. (***$P < 0.001$; **$P < 0.01$; *$P < 0.05$).

E Western blot analysis of proteins recovered in cytoplasmic (CY) nuclear soluble (NS) and nuclear matrix (NM) fractions (upper panels) of MCF7 cells treated or not with 0.5 μM of rotenone for 1 h (as indicated). Graph (bottom panel) represents the quantitative analysis of SAFB in immunoblots (soluble and nuclear matrix fractions) after the indicated treatment. Columns represent the mean of two independent experiments ±s.e.m. (n = 2; *P < 0.05).

and regulates their function. Indeed, analysis of the SAFB1/2 immunoprecipitates by Western blotting confirmed that the association of both SRPK1 and the SR-splicing factor SF2 with SAFB1/2 was impaired after the short-term exposure of the cells to hypoxia (Fig. 4F).

Moreover, MS analysis of the immunoprecipitated SAFB1/2 revealed the presence of peptides containing oxidized methionine (methionine sulfoxide) residues specifically under hypoxia (Table S1) and at similar positions inside the amino acid sequences of SAFB1 and SAFB2 (Fig. 4G), suggesting that the changes in the SAFB1/2 interactome under hypoxia are the result SAFB1/2 oxidation, which is probably triggered by the increased ROS production upon oxygen deprivation.

3.5. Short-term hypoxia induces ROS- and SAFB1/2-dependent remodeling of the splicing machinery

SAFB interacting proteins SF2 and SRPK1 are both major regulators of the splicing machinery and are also both controlled by SAFBs [14]. SF2 belongs to the family of SR splicing factors characterized by RS-dipeptide motives, the phosphorylation of which regulates their localization and their function in constitutive and alternative splicing [16]. Analysis using mab104 that specifically recognizes the phosphorylated RS motif [37] showed that SR-protein phosphorylation was reduced by short-term exposure of MCF7 cells to hypoxia (Fig. 5A). Furthermore, analysis of SF2 immunoprecipitates confirmed both the reduction of its phosphorylation as well as the inhibition of its association with SAFB under hypoxia (Fig. 5B). SF2 phosphorylation controls its migration from nuclear speckles to the active spliceosomes [14,16].

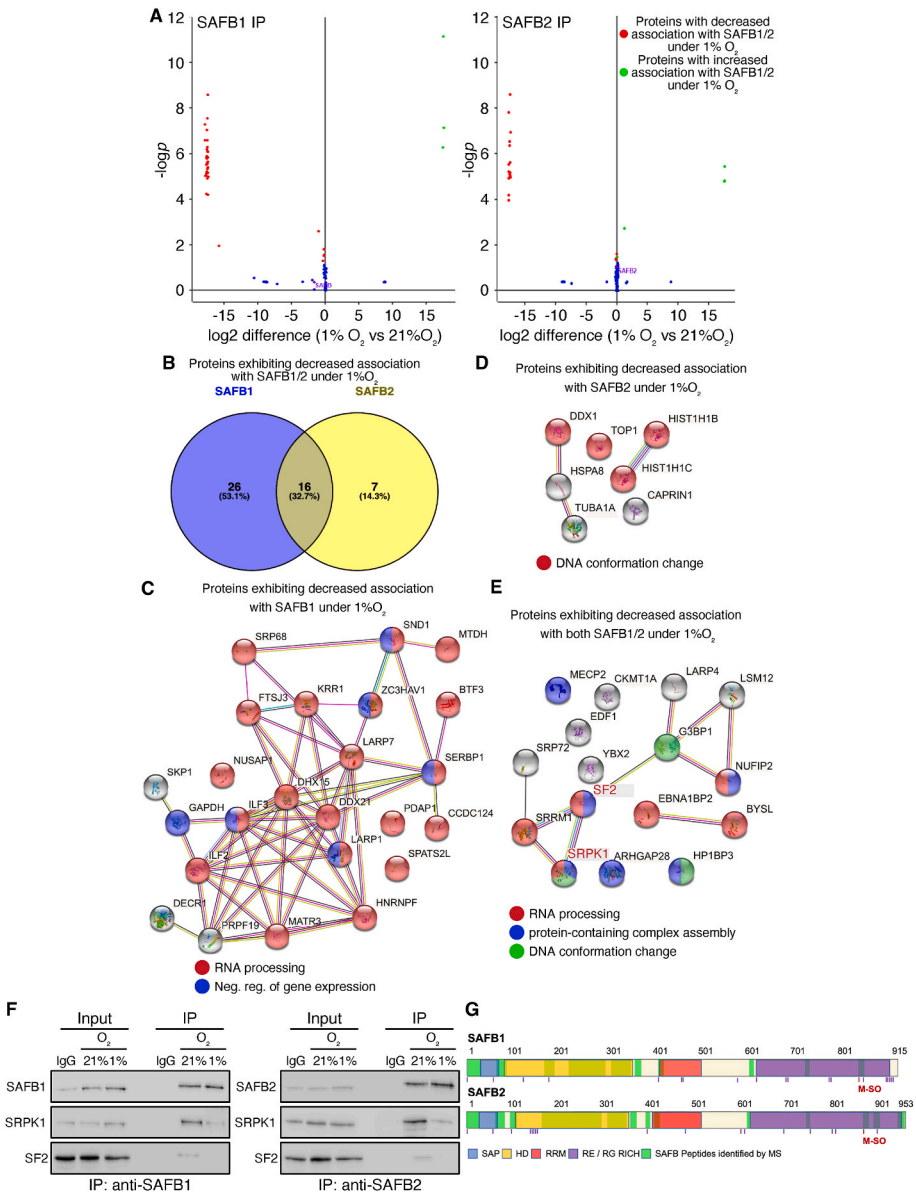

Fig. 4. Short-term hypoxia abolishes the association of SAFB1/2 with essential components of splicing machinery and chromatin organization.

A Volcano plots of proteins showing significantly altered association with SAFB1 (left panel) or SAFB2 (right panel) in MCF7 cells kept in 21% O_2 or 1% O_2 after mass spectrometry analysis of anti-SAFB1 or anti-SAFB2 immunoprecipitates. Graphs depict the difference between the two samples expressed as log2 (x) versus their statistical significance expressed as –Log10(p-value) from two biological replicates ($P < 0.05$). SAFB1/2 levels are shown in purple.

B Venn diagram showing the number of proteins exhibiting decreased association with either SAFB1 (magenta) or SAFB2 (yellow) under 1% O_2.

C-E STRING analysis depicting the different clusters of proteins (as indicated) showing decreased association with either SAFB1 (**C**), SAFB2 (**D**), or both SAFB1/2 (**E**), and under 1% O_2. Biological functions are indicated by color as shown. Gene names corresponding to proteins further verified by immunoblotting are indicated in color.

F Protein extracts (INPUTS) or anti-SAFB1 (left panels)/anti-SAFB2 (right panels) immunoprecipitates (IP) of MCF7 cells grown at 21% or 1% O_2 for 2 h were analyzed using antibodies against the indicated proteins. Images are representative of two independent experiments.

G Schematic representation of SAFB1 and SAFB2 domains (as indicated; *SAP*: SAF-A/B, Acinus and PIAS, *HD*: Homology Domain, *RRM*: RNA Recognition Motif, *RE/RG*: Arginine-Glutamate/Arginine-Glycine) and SAFB1/2 peptides identified by mass spectrometry (Green). Methionine residues (oxidized shown in Red or not shown as vertical Magenta lines) are also indicated in their respective positions.

Indeed, microscopical examination of nuclear SF2 distribution revealed that short exposure of cells to 1% O_2 affected both the size and number of intranuclear SF2 foci (Fig. S6A), assumingly as a result of its reduced modification by SRPK1. This is further supported by the effects of hypoxia on SRPK1 itself, which included its reduced interaction with both SAFB and SF2 (Figs. 4F and 5B) accompanied by its migration from the nucleus to the cytoplasm (Fig. 5D), as well as its increased association with cytoplasmic [38] hsp70-containing structures (Fig. S6B). These changes were concomitant with the dissociation of SF2 from the nuclear matrix and its migration towards soluble nuclear fractions, as documented by subcellular fractionation (Fig. 5C) and immunofluorescence microscopy (Fig. S6A). Interestingly, treatment of the hypoxic cells with the antioxidant NAC restored the levels of nuclear SRPK1 (Fig. 5C and D) and also recovered the SF2 ratio from soluble to nuclear matrix fractions (Fig. 5C), suggesting that the observed changes of the splicing machinery under hypoxia are linked to the ROS-dependent intranuclear SAFB1/2 redistribution and maybe result in the reprogramming of VEGF mRNA splicing and stimulation of the proangiogenic VEGFa variant synthesis, as described above.

In support of this hypothesis, depletion of SAFB1/2 under normoxia phenocopied the hypoxic shift in favor of the proangiogenic VEGFa form, while SAFB1/2 depletion under hypoxia had no significant effect on the balance between the two VEGF mRNA forms (Fig. 5E and Fig. S6C). Finally, treatment of MCF7 cells with the antioxidant NAC (Fig. 5F) or SF2 depletion (Figs. S6D and S6E) under hypoxia also restored the normoxic phenotype in terms of VEGF mRNA splicing balance. Conversely, treating normoxic MCF7 cells with rotenone caused a significant increase in VEGFa levels much like hypoxia (Fig. 5G). In summary, our data support a causative link between the hypoxia-induced effects on the SAFB1/2-SRPK1-SF2 axis and VEGF mRNA alternative splicing.

4. Discussion

The development of a hypoxic microenvironment is a common trait of solid tumors in which cancer cell adaptation to low oxygen is mainly driven via HIF-α stabilization and subsequent activation of the HIF gene targets [1]. Another feature of cancer cells is alternative or aberrant splicing of nascent pre-mRNA molecules that facilitates tumor growth [39,40]. A prominent example is the splicing of the *VEGFA* transcript that can either produce the VEGFa isoform, having pro-angiogenic abilities and is frequently encountered in human cancers, and the

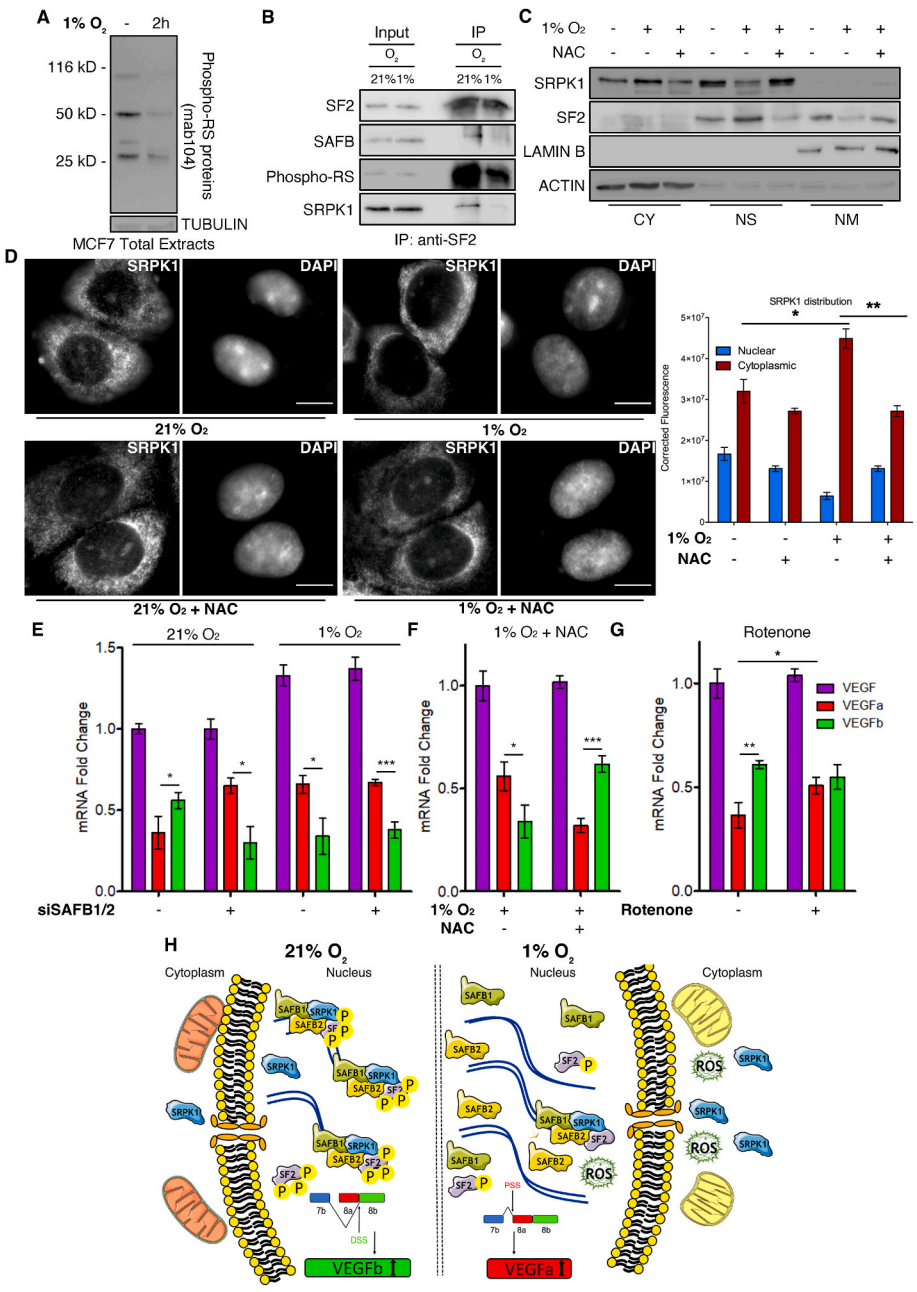

Fig. 5. Short-term hypoxia induces ROS- and SAFB1/2-dependent remodeling of the splicing machinery.

A Western blot analysis exhibiting the phosphorylated RS-protein levels in total extracts of MCF cells incubated under 21% or 1% O_2 for 2 h.

B Protein extracts (INPUTS) or anti-SF2 immunoprecipitates (IP) of MCF7 cells grown at 21% or 1% O_2 for 2 h were analyzed using antibodies against the indicated proteins or modifications. Images are representative of three independent experiments (A and B).

C SRPK1 and SF2 immunoblotting in subcellular fractions (CY: Cytoplasmic fraction, NS: Nuclear Soluble fraction, NM: insoluble Nuclear Matrix fraction) of MCF-7 cells incubated at 21% or 1% O_2 for 2 h and in the presence or not of 1 mM NAC (as indicated). Actin and Lamin B were used as fractionation control. Blots are representative of two independent experiments.

D Immunofluorescence microscopy images of MCF7 cells grown on coverslips at 21% or 1% O_2 for 2 h using antibodies against SRPK1 and treated or not with 1 mM NAC (As indicated). Nuclei were stained with DAPI (Scale bars: 10 μM). Graph (right panel) represents the quantification of SRPK1 cytoplasmic vs nuclear signal as corrected fluorescence intensity from a total of 40 individual cells from two independent experiments in each condition ±s.e.m. (**P < 0.01; *P < 0.05).

E mRNA fold change levels of total *VEGFA* (magenta) or its alternatively spliced forms (VEGFa: red; VEGFb: green) determined by RT-PCR in MCF-7 cells incubated at 21% or 1% O_2 for 2 h and treated or not with siRNA for both SAFB1/2 (as indicated). Results are shown as the ratio in relation to the total *VEGFA* levels in normoxia and represent the mean of three independent experiments performed in triplicates ± s.d. (n = 9; ***$P < 0.001$; *$P < 0.05$).

F mRNA fold change levels of total *VEGFA* (magenta) or its alternatively spliced forms (VEGFa: red; VEGFb: green) determined by RT-PCR in MCF-7 cells incubated at 1% O_2 for 2 h and treated or not with 1 mM NAC (as indicated). Results are shown as ratios in relation to the total *VEGFA* levels in hypoxia and represent the mean of three independent experiments performed in triplicates ± s.d. (n = 9; ***$P < 0.001$; *$P < 0.05$).

G mRNA fold change levels of total *VEGFA* (magenta) or its alternatively spliced forms (VEGFa: red; VEGFb: green) determined by RT-PCR in MCF-7 cells treated or not with 0.5 μM of rotenone for 30 min (as indicated). Results are shown as ratios in relation to the total *VEGFA* levels in normoxia and represent the mean of three independent experiments performed in triplicates ± s.d. (n = 9; **$P < 0.01$; *$P < 0.05$).

H Model depicting the involvement of SAFB1/2 and ROS in regulating the splicing machinery under hypoxia. When oxygen is ample SAFB1/2 proteins populate the nuclear matrix and show increased association with components of splicing machinery such as SF2 and SRPK1 (left panel). When oxygen is sparse (right panel), ROS are produced due to mitochondrial disfunction. SAFB1/2 dissociate from the nuclear matrix and show reduced affinity for splicing components. This splicing machinery remodeling shifts the balance towards a proangiogenic VEGF form under hypoxia.

anti-angiogenic VEGFb form predominantly expressed in healthy human tissues [9]. Hypoxia, in addition to inducing total *VEGFA* mRNA levels and affecting its stability [41] has also been shown to influence its alternative splicing [10,11]. However, the relevant studies on *VEGFA* mRNA splicing were performed at late time points, not excluding the direct or indirect role of HIF-mediated transcriptional products. We have now shown that the switch between the VEGFa and VEGFb forms occurs when cells are exposed to hypoxia for a short period (less than 2 h), which is not sufficient for significant upregulation of hypoxia target gene expression as also previously shown in different model systems including MCF7 cells [42,43]. Indeed, at this time point, we observed no significant changes in total *VEGFA* mRNA levels (indicative of HIF activity). Additionally, under the same conditions, total mRNA levels of two established HIF-1 targets (*LDHA* and *BNIP3*) remained relatively unaltered. At the same time, the level of the fully functional LDHA-001 variant increased [10] while there was a significant downregulation of BNIP3ΔEx2 that carries a premature termination codon [31], suggestive of a broader role for alternative splicing on cancer cell survival at the

onset of hypoxia. Furthermore, the hypoxic switch in *VEGFA* splicing was also confirmed in a HeLa cell line lacking both HIF-α isoforms. Having ruled out any HIF involvement, our data point to the rapid subnuclear SAFB1/2 redistribution as the trigger for shifting the balance in favor of a VEGF splice variant that can facilitate adaptation to hypoxia by stimulating angiogenesis. Summarizing our results, we have provided evidence that: (i) under normal oxygen conditions, SAFB1/2 proteins mostly populate the nuclear matrix and show increased association with components of splicing machinery such as SF2 and SRPK1; (ii) reduced oxygen availability quickly leads to enhanced ROS production due to mitochondrial dysfunction, which in turn causes dissociation of SAFB1/2 from the nuclear matrix and reduced affinity for major constituents of the splicing apparatus; (iii) this SAFB1/2- and ROS-dependent remodeling of the splicing machinery/nuclear matrix interface shifts the balance towards the production of the pro-angiogenic VEGF form that is negated after treatment with NAC or SF2 silencing.

The nuclear matrix is often thought of as a rigid subnuclear structure that supports chromatin. In reality, however, the dynamic nature of the nuclear matrix, mostly involving the SAFB1/2 proteins [18], is essential for the flexibility of the nuclear functional and topological architecture in response to various conditions. Indeed, SAFB1/2, initially identified by their ability to bind Scaffold/Matrix attachment regions (SAR/MAR) of DNA elements [44], have been subsequently shown to be involved through their DNA/RNA- and protein-binding abilities in many processes including gene regulation [21], stress response [23], DNA repair [22], heterochromatin stabilization [20] and regulation of mRNA processing and splicing [18,45,46].

Our proteomic analysis has further expanded the latter notion by showing that both SAFB1 and SAFB2 can form complexes with mRNA splicing-associated factors (ribonucleoproteins, SR-proteins, and their kinase) in a dynamic fashion regulated by oxygen availability and intracellular ROS production. Furthermore, our proteomic analysis has revealed that SAFB1/2 undergo methionine oxidation at specific sites only under hypoxic conditions. The oxidized methionine residues are confined in the C-terminal domain of SAFB1/2, which is likely unstructured and is responsible for many of its protein-protein interactions [18]. Although methionine oxidation observed by MS may be a random effect of sample preparation, the fact that the SAFB1/2 modified residues were only detected in samples derived from hypoxic cells and in similar positions in both SAFB isoforms strongly suggests that this modification had occurred intracellularly. It has indeed been previously shown that exposed methionine residues found in intrinsically disordered protein domains can be oxidized by endogenous ROS production [47] and under conditions including exposure of cells to brief bursts of hypoxia/reoxygenation [48]. As methionine oxidation can be easily reversed by methionine sulfoxide reductases [49], the introduction of this modification into key signaling or structural proteins may provide the means for a very fast response to conditions affecting the intracellular oxidoreductive balance such as the rapid production of ROS at the onset of hypoxia. Our results have demonstrated that the protein-protein interactions involving SAFB1/2 are indeed quickly responsive to alterations in oxygen concentration. The flexible nature of SAFB1/2 associations has also been shown previously in response to heat stress, with SAFB1 forming large nuclear stress bodies [50], pro-apoptotic signaling, with SAFB1 forming peri-nucleolar structures [51], or 1,6-hexanediol, which abolished the ability of SAFB1 to drive phase separation in nuclear foci [20]. Furthermore, and in agreement with previous studies [17,20,46], our interactome analysis suggests that SAFB1 and SAFB2, despite their highly similar structure and shared associations, also possess distinct roles, with SAFB1 exhibiting preferential affinity for gene expression regulators whereas SAFB2 shows higher affinity for proteins associated with alterations of DNA structure.

We have also shown that two prominent splicing regulators, SF2 and SRPK1, both implicated in pro-carcinogenic alternative splicing [9,12], are among the splicing machinery components that dissociate from SAFB1/2 and concomitantly show altered localization in nuclear soluble and cytoplasmic fractions under hypoxia in a process largely reversed by the antioxidant NAC. SF2, a product of the *SRSF1* gene, is frequently overexpressed in human cancers, and it promotes alternative splicing of pre-mRNAs in breast cancer cells [52]. SF2 overexpression has also been shown to promote the inclusion of exon 8a upon VEGF mRNA splicing, thus producing the pro-angiogenic VEGFa variant, whereas SRSF6 promotes the inclusion of exon 8b, producing the anti-angiogenic VEGFb form [9]. According to our results, although SF2 expression is not increased after short-term hypoxic treatment, its release from SAFB1/2 could increase its availability, thereby promoting proximal splice site selection and VEGFa production, as also observed in hypoxic tumors [40]. We could additionally show that shifting the balance towards the pro-angiogenic VEGF form can also be achieved by silencing the expression of SAFB1/2 or rotenone treatment under normoxia, which phenocopy SAFB1/2 removal from the nuclear matrix under hypoxia. In agreement, lower SAFB levels have been associated with adverse outcome for breast cancer patients [53].

Splice site selection in VEGF mRNA can also be affected by SRPK1-mediated phosphorylation of the SF2 RS/SR-dipeptide stretch [12,54]. Temporal regulation of the level of RS-motif phosphorylation in SR-proteins is important because phosphorylation of splicing factors mediates spliceosome assembly, but their dephosphorylation is essential for the progression of the spliceosome to the catalysis mRNA splicing reactions and subsequent mRNA nuclear export [14,16].

Our results show that the high phosphorylation level of SR-proteins and SF2 observed under normoxia is quickly diminished upon oxygen deprivation, although it still remains substantial, possibly to facilitate both site selection and reaction efficiency. These changes in phosphorylation levels mostly rely on the control of SRPK1 subcellular localization. Although steady-state localization of SRPKs is mostly cytoplasmic with a smaller nuclear fraction, nucleo-cytoplasmic shuttling of SRPKs is important for controlling cellular processes [16] and for conferring resistance to cisplatin and 5-FU [15,55]. More specifically, regulation of SRPK1 nucleo-cytoplasmic shuttling is complex and involves its intramolecular structure [56,57], its post-translational modifications [15,55] and, especially, its protein-protein interactions [16,17,19]. As previously shown, a fraction of nuclear SRPK1 is associated with the nuclear matrix as a result of its binding to SAFB1/2 [19] and the formation of a trimeric complex between SAFBs/SRPK1 and ERH that controls SRPK1 catalytic activity [17]. Our data suggest that the hypoxia apart from causing the dissociation of SRPK1 from SAFB1/2 also leads to its ROS-inducible translocation to the cytoplasm, in agreement with the concomitant general reduction in RS phosphorylation. Accordingly, SRPK1-mediated phosphorylation sequesters splicing factor RBM4 in the cytoplasm and favors the expression of an anti-apoptotic MCL-1 form in MCF7 cells [58].

To conclude, our results can be summarized in the following proposed model (Fig. 5H): SAFB1/2, by associating with both splicing factors and their modifying kinase, can act as a rheostat that regulates both splicing factor availability at active splice sites and their phosphorylation level. When oxygen levels drop, the rapid ROS-mediated oxidation of SAFBs and the subsequent dissociation of nuclear matrix-anchored complexes ensures that more free SF2 molecules become immediately available inside the nucleus and that nuclear SRPK1 is translocated to the cytoplasm. These events finely tune the level of SR-protein phosphorylation and promote pro-angiogenic VEGFa formation under hypoxia. This is an immediate and early response to hypoxia driven by and increased and transient ROS production as a result of deregulated mitochondrial respiration as soon as oxygen levels fall [34]. When hypoxia persists, or in cells in which the initial burst of ROS production does not occur at the onset of hypoxia, stabilization of HIF-α and activation of HIF-mediated transcription can take over by enabling the expression of proteins that neutralize ROS [34,36,59,60], readjust the electron transport chain [35], and promote alternative and adaptive mRNA splicing [9,10,12].

Data availability

The proteomic data discussed in this publication have been deposited to the ProteomeXchange Consortium (http://proteomecentral.proteomexchange.org) via the PRIDE partner repository [61] with the dataset identifier no: PXD030933.

Requests for materials should be addressed to E.G. and I.M.

Funding

This research is co-financed by Greece and the European Union (European Social Fund- ESF) through the Operational Programme « Human Resources Development, Education and Lifelong Learning» in the context of the project "Strengthening Human Resources Research Potential via Doctorate Research" (MIS-5000432), implemented by the State Scholarships Foundation (IKY) fellowship to C.T.

I.M. would like to thank Fondation Santé for their financial support. This work was partially supported by the Hellenic Foundation for Research and Innovation (H.F.R.I.) under the "First Call for H.F.R.I. Research Projects to support Faculty members and Researchers and the procurement of high-cost research equipment grant" (Project Number: HFRI-FM17-2132 to I.M.).

Author contributions

C.T. performed experiments, analysis, and paper writing, S.D.: performed experiments, M.S. and G.P.: Proteomic Analysis, G.S., E.G. and I.M.: design and paper writing, I.M. analysis, supervision, and funding.

Declaration of competing interest

The authors declare that they have no conflict of interest.

Acknowledgments

We are grateful to Prof. Jamal Tazi (University of Montpellier, France) for providing mab104 antisera. We also thank Dr. P. Moutsatsou (Medical School, University of Athens, Greece) for providing us with the MCF-7 cells originally acquired from ATCC and Prof. Antonis Koromilas (McGill University, Canada), and Dr. Ioannis Sanidas (Roswell Park Comprehensive Cancer Center, USA) for their useful comments and discussions on the manuscript.

Appendix A. Supplementary data

Supplementary data to this article can be found online at https://doi.org/10.1016/j.redox.2022.102545.

References

[1] G.L. Semenza, Pharmacologic targeting of hypoxia-inducible factors, Annu. Rev. Pharmacol. Toxicol. 59 (2019) 379–403.
[2] L. Schito, G.L. Semenza, Hypoxia-inducible factors: master regulators of cancer progression, Trends Cancer 2 (12) (2016) 758–770.
[3] Z. Andrysik, H. Bender, M.D. Galbraith, J.M. Espinosa, Multi-omics analysis reveals contextual tumor suppressive and oncogenic gene modules within the acute hypoxic response, Nat. Commun. 12 (1) (2021) 1375.
[4] M. Batie, J. Frost, M. Frost, J.W. Wilson, P. Schofield, S. Rocha, Hypoxia induces rapid changes to histone methylation and reprograms chromatin, Science 363 (6432) (2019) 1222–1226.
[5] A.A. Chakraborty, T. Laukka, M. Myllykoski, A.E. Ringel, M.A. Booker, M. Y. Tolstorukov, Y.J. Meng, S.R. Meier, R.B. Jennings, A.L. Creech, Z.T. Herbert, S. K. McBrayer, B.A. Olenchock, J.D. Jaffe, M.C. Haigis, R. Beroukhim, S. Signoretti, P. Koivunen, W.G. Kaelin Jr., Histone demethylase KDM6A directly senses oxygen to control chromatin and cell fate, Science 363 (6432) (2019) 1217–1222.
[6] A. Swaminathan, D. Kasiviswanathan, U.M. Balaguru, G.K. Kolluru, G. SuryaKumar, S. Chatterjee, Hypoxia perturbs endothelium by re-organizing cellular actin architecture: nitric oxide offers limited protection, Tissue Cell 50 (2018) 114–124.
[7] M. Koritzinsky, M.l.G. Magagnin, T.v.d. Beucken, R. Seigneuric, K. Savelkouls, J. e. Dostie, S.p. Pyronnet, R.J. Kaufman, S.A. Weppler, J.W. Voncken, P. Lambin, C. Koumenis, N. Sonenberg, B.G. Wouters, Gene expression during acute and prolonged hypoxia is regulated by distinct mechanisms of translational control, EMBO J. 25 (2006) 1114–1125.
[8] P.P. Coltri, M.G.P. Dos Santos, G.H.G. da Silva, Splicing and cancer: challenges and opportunities, Wiley Interdiscip Rev RNA 10 (3) (2019), e1527.
[9] L.M. Urbanski, N. Leclair, O. Anczukow, Alternative-splicing defects in cancer: splicing regulators and their downstream targets, guiding the way to novel cancer therapeutics, Wiley Interdiscip Rev RNA 9 (4) (2018), e1476.
[10] J. Han, J. Li, J.C. Ho, G.S. Chia, H. Kato, S. Jha, H. Yang, L. Poellinger, K.L. Lee, Hypoxia is a key driver of alternative splicing in human breast cancer cells, Sci. Rep. 7 (1) (2017) 4108.
[11] D. Zhang, Y. Duan, J. Cun, Q. Yang, Identification of prognostic alternative splicing signature in breast carcinoma, Front. Genet. 10 (2019) 278.
[12] A.R. Farina, L. Cappabianca, M. Sebastiano, V. Zelli, S. Guadagni, A.R. Mackay, Hypoxia-induced alternative splicing: the 11th hallmark of cancer, J. Exp. Clin. Cancer Res. 39 (1) (2020) 110.
[13] M.A. Rahman, F. Nasrin, S. Bhattacharjee, S. Nandi, Hallmarks of splicing defects in cancer: clinical applications in the era of personalized medicine, Cancers 12 (6) (2020).
[14] T. Giannakouros, E. Nikolakaki, I. Mylonis, E. Georgatsou, Serine-arginine protein kinases: a small protein kinase family with a large cellular presence, FEBS J. 278 (4) (2011) 570–586.
[15] C. Wang, Z. Zhou, C.S. Subhramanyam, Q. Cao, Z.S.L. Heng, W. Liu, X. Fu, Q. Hu, SRPK1 acetylation modulates alternative splicing to regulate cisplatin resistance in breast cancer cells, Commun. Biol. 3 (1) (2020) 268.
[16] X.Y. Zhong, P. Wang, J. Han, M.G. Rosenfeld, X.D. Fu, SR proteins in vertical integration of gene expression from transcription to RNA processing to translation, Mol. Cell 35 (1) (2009) 1–10.
[17] S. Drakouli, A. Lyberopoulou, M. Papathanassiou, I. Mylonis, E. Georgatsou, Enhancer of rudimentary homologue interacts with scaffold attachment factor B at the nuclear matrix to regulate SR protein phosphorylation, FEBS J. 284 (15) (2017) 2482–2500.
[18] M. Norman, C. Rivers, Y.B. Lee, J. Idris, J. Uney, The increasing diversity of functions attributed to the SAFB family of RNA-/DNA-binding proteins, Biochem. J. 473 (23) (2016) 4271–4288.
[19] D. Tsianou, E. Nikolakaki, A. Tzitzira, S. Bonanou, T. Giannakouros, E. Georgatsou, The enzymatic activity of SR protein kinases 1 and 1a is negatively affected by interaction with scaffold attachment factors B1 and 2, FEBS J. 276 (18) (2009) 5212–5227.
[20] X. Huo, L. Ji, Y. Zhang, P. Lv, X. Cao, Q. Wang, Z. Yan, S. Dong, D. Du, F. Zhang, G. Wei, Y. Liu, B. Wen, The nuclear matrix protein SAFB cooperates with major satellite RNAs to stabilize heterochromatin architecture partially through phase separation, Mol. Cell 77 (2) (2020) 368–383 e7.
[21] S. Oesterreich, T.M. Sullivan, S.K. Samuel, J.R. Davie, S.A. Fuqua, Novel nuclear matrix protein HET binds to and influences activity of the HSP27 promoter in human breast cancer cells, J. Cell. Biochem. 67 (2) (1997) 275–286.
[22] M. Altmeyer, L. Toledo, T. Gudjonsson, M. Grofte, M.B. Rask, C. Lukas, V. Akimov, B. Blagoev, J. Bartek, J. Lukas, The chromatin scaffold protein SAFB1 renders chromatin permissive for DNA damage signaling, Mol. Cell 52 (2) (2013) 206–220.
[23] G. Biamonti, C. Vourc'h, Nuclear stress bodies, Cold Spring Harbor Perspect. Biol. 2 (6) (2010), a000695.
[24] I. Mylonis, G. Chachami, M. Samiotaki, E. Georgatsou, S. Bonanou, G. Simos, Identification of MAPK phosphorylation sites and their role in the localization and activity of hypoxia-inducible factor-1α, J. Biol. Chem. 281 (44) (2006) 33095–33106.
[25] S. Tyanova, T. Temu, P. Sinitcyn, A. Carlson, M.Y. Hein, T. Geiger, M. Mann, J. Cox, The Perseus computational platform for comprehensive analysis of (prote) omics data, Nat. Methods 13 (9) (2016) 731–740.
[26] D. Mellacheruvu, Z. Wright, A.L. Couzens, J.P. Lambert, N.A. St-Denis, T. Li, Y. V. Miteva, S. Hauri, M.E. Sardiu, T.Y. Low, V.A. Halim, R.D. Bagshaw, N.C. Hubner, A. Al-Hakim, A. Bouchard, D. Faubert, D. Fermin, W.H. Dunham, M. Goudreault, Z. Y. Lin, B.G. Badillo, T. Pawson, D. Durocher, B. Coulombe, R. Aebersold, G. Superti-Furga, J. Colinge, A.J. Heck, H. Choi, M. Gstaiger, S. Mohammed, I. M. Cristea, K.L. Bennett, M.P. Washburn, B. Raught, R.M. Ewing, A.C. Gingras, A. I. Nesvizhskii, The CRAPome: a contaminant repository for affinity purification-mass spectrometry data, Nat. Methods 10 (8) (2013) 730–736.
[27] J.C. Oliveros, Venny, An interactive tool for comparing lists with Venn's diagrams, 2015, https://bioinfogp.cnb.csic.es/tools/venny/index.html, 2007.
[28] S.X. Ge, D. Jung, R. Yao, ShinyGO: a graphical gene-set enrichment tool for animals and plants, Bioinformatics 36 (8) (2020) 2628–2629.
[29] D. Szklarczyk, A.L. Gable, K.C. Nastou, D. Lyon, R. Kirsch, S. Pyysalo, N. T. Doncheva, M. Legeay, T. Fang, P. Bork, L.J. Jensen, C. von Mering, The STRING database in 2021: customizable protein-protein networks, and functional characterization of user-uploaded gene/measurement sets, Nucleic Acids Res. 49 (D1) (2021) D605–D612.
[30] R.A. McCloy, S. Rogers, C.E. Caldon, T. Lorca, A. Castro, A. Burgess, Partial inhibition of Cdk1 in G 2 phase overrides the SAC and decouples mitotic events, Cell Cycle 13 (9) (2014) 1400–1412.
[31] J.T. Field, M.D. Martens, W. Mughal, Y. Hai, D. Chapman, G.M. Hatch, T.L. Ivanco, W. Diehl-Jones, J.W. Gordon, Misoprostol regulates Bnip3 repression and alternative splicing to control cellular calcium homeostasis during hypoxic stress, Cell Death Dis. 4 (2018) 37.
[32] E. Nikolakaki, R. Kohen, A.M. Hartmann, S. Stamm, E. Georgatsou, T. Giannakouros, Cloning and characterization of an alternatively spliced form of SR protein kinase 1 that interacts specifically with scaffold attachment factor-B, J. Biol. Chem. 276 (43) (2001) 40175–40182.

[33] K. Koukoulas, A. Giakountis, A. Karagiota, M. Samiotaki, G. Panayotou, G. Simos, I. Mylonis, ERK signaling controls productive HIF-1 binding to chromatin and cancer cell adaptation to hypoxia through HIF-1alpha interaction with NPM1, Mol. Oncol. 15 (12) (2021) 3468–3489.
[34] L.W. Thomas, M. Ashcroft, Exploring the molecular interface between hypoxia-inducible factor signalling and mitochondria, Cell. Mol. Life Sci. 76 (9) (2019) 1759–1777.
[35] R. Fukuda, H. Zhang, J.W. Kim, L. Shimoda, C.V. Dang, G.L. Semenza, HIF-1 regulates cytochrome oxidase subunits to optimize efficiency of respiration in hypoxic cells, Cell 129 (1) (2007) 111–122.
[36] P. Lee, N.S. Chandel, M.C. Simon, Cellular adaptation to hypoxia through hypoxia inducible factors and beyond, Nat. Rev. Mol. Cell Biol. 21 (5) (2020) 268–283.
[37] E. Labourier, H.-M. Bourbon, I.-e. Gallouzi, M. Fostier, E. Allemand, J. Tazi, Antagonism between RSF1 and SR proteins for both splice-site recognition in vitro and Drosophila development, Genes Dev. 13 (1999) 740–753.
[38] Z. Zhou, J. Qiu, W. Liu, Y. Zhou, R.M. Plocinik, H. Li, Q. Hu, G. Ghosh, J.A. Adams, M.G. Rosenfeld, X.D. Fu, The Akt-SRPK-SR axis constitutes a major pathway in transducing EGF signaling to regulate alternative splicing in the nucleus, Mol. Cell 47 (3) (2012) 422–433.
[39] A. Yoshimi, K.T. Lin, D.H. Wiseman, M.A. Rahman, A. Pastore, B. Wang, S.C. Lee, J. B. Micol, X.J. Zhang, S. de Botton, V. Penard-Lacronique, E.M. Stein, H. Cho, R. E. Miles, D. Inoue, T.R. Albrecht, T.C.P. Somervaille, K. Batta, F. Amaral, F. Simeoni, D.P. Wilks, C. Cargo, A.M. Intlekofer, R.L. Levine, H. Dvinge, R. K. Bradley, E.J. Wagner, A.R. Krainer, O. Abdel-Wahab, Coordinated alterations in RNA splicing and epigenetic regulation drive leukaemogenesis, Nature 574 (7777) (2019) 273–277.
[40] C.J. David, J.L. Manley, Alternative pre-mRNA splicing regulation in cancer: pathways and programs unhinged, Genes Dev. 24 (21) (2010) 2343–2364.
[41] A.P. Levy, N.S. Levy, M.A. Goldberg, Post-transcriptional regulation of vascular endothelial growth factor by hypoxia, J. Biol. Chem. 271 (5) (1996) 2746–2753.
[42] M. Salton, T.C. Voss, T. Misteli, Identification by high-throughput imaging of the histone methyltransferase EHMT2 as an epigenetic regulator of VEGFA alternative splicing, Nucleic Acids Res. 42 (22) (2014) 13662–13673.
[43] R. Bartoszewski, A. Moszyńska, M. Serocki, A. Cabaj, A. Polten, R. Ochocka, L. Dell'Italia, S. Bartoszewska, J. Króliczewski, M. Dąbrowski, J.F. Collawn, Primary endothelial cell-specific regulation of hypoxia-inducible factor (HIF)-1 and HIF-2 and their target gene expression profiles during hypoxia, Faseb. J. 33 (7) (2019) 7929–7941.
[44] A. Renz, O. Fackelmayer, Purification and molecular cloning of the scaffold attachment factor B (SAF-B), a novel human nuclear protein that specifically binds to S/MAR-DNA, Nucleic Acids Res. 24 (5) (1996) 843–849.
[45] W.S. Oliver Nayler, Jean-Pierre Bourquin, Igor Stagljar, Lothar Lindemann, A.M. H. Heinrich Jasper, Frank O. Fackelmayer, Axel Ullrich, S. Stamm, SAF-B protein couples transcription and pre-mRNA splicing to SAR/MAR elements, Nucleic Acids Res. 26 (15) (1998) 3542–3549.
[46] K.A. Sergeant, C.F. Bourgeois, C. Dalgliesh, J.P. Venables, J. Stevenin, D.J. Elliott, Alternative RNA splicing complexes containing the scaffold attachment factor SAFB2, J. Cell Sci. 120 (2007) 309–319.
[47] E.J. Walker, J.Q. Bettinger, K.A. Welle, J.R. Hryhorenko, S. Ghaemmaghami, Global analysis of methionine oxidation provides a census of folding stabilities for the human proteome, Proc. Natl. Acad. Sci. U. S. A. 116 (13) (2019) 6081–6090.
[48] O. Yermolaieva, R. Xu, C. Schinstock, N. Brot, H. Weissbach, S.H. Heinemann, T. Hoshi, Methionine sulfoxide reductase A protects neuronal cells against brief hypoxia/reoxygenation, Proc. Natl. Acad. Sci. U. S. A. 101 (5) (2004) 1159–1164.
[49] T. Hoshi, S. Heinemann, Regulation of cell function by methionine oxidation and reduction, J. Physiol. 531 (Pt 1) (2001) 1–11.
[50] F. Weighardt, F. Cobianchi, L. Cartegni, I. Chiodi, A. Villa, S. Riva, G. Biamonti, A novel hnRNP protein (HAP/SAF-B) enters a subset of hnRNP complexes and relocates in nuclear granules in response to heat shock, J. Cell Sci. 112 (1999) 1465–1476.
[51] Y.B. Lee, S. Colley, M. Norman, G. Biamonti, J.B. Uney, SAFB re-distribution marks steps of the apoptotic process, Exp. Cell Res. 313 (18) (2007) 3914–3923.
[52] O. Anczukow, M. Akerman, A. Clery, J. Wu, C. Shen, N.H. Shirole, A. Raimer, S. Sun, M.A. Jensen, Y. Hua, F.H. Allain, A.R. Krainer, SRSF1-Regulated alternative splicing in breast cancer, Mol. Cell 60 (1) (2015) 105–117.
[53] S. Hammerich-Hille, V.J. Bardout, S.G. Hilsenbeck, C.K. Osborne, S. Oesterreich, Low SAFB levels are associated with worse outcome in breast cancer patients, Breast Cancer Res. Treat. 121 (2) (2010) 503–509.
[54] D.G. Nowak, J. Woolard, E.M. Amin, O. Konopatskaya, M.A. Saleem, A. J. Churchill, M.R. Ladomery, S.J. Harper, D.O. Bates, Expression of pro- and anti-angiogenic isoforms of VEGF is differentially regulated by splicing and growth factors, J. Cell Sci. 121 (Pt 20) (2008) 3487–3495.
[55] I. Sigala, M. Koutroumani, A. Koukiali, T. Giannakouros, E. Nikolakaki, Nuclear translocation of SRPKs is associated with 5-FU and cisplatin sensitivity in HeLa and T24 cells, Cells 10 (4) (2021).
[56] I. Sanidas, V. Kotoula, E. Ritou, J. Daans, C. Lenz, M. Mairhofer, M. Daniilidou, A. Kolbus, V. Kruft, P. Ponsaerts, E. Nikolakaki, The ratio of SRPK1/SRPK1a regulates erythroid differentiation in K562 leukaemic cells, Biochim. Biophys. Acta 1803 (12) (2010) 1319–1331.
[57] M. Koutroumani, G.E. Papadopoulos, M. Vlassi, E. Nikolakaki, T. Giannakouros, Evidence for disulfide bonds in SR Protein Kinase 1 (SRPK1) that are required for activity and nuclear localization, PLoS One 12 (2) (2017), e0171328.
[58] J.C. Lin, C.Y. Lin, W.Y. Tarn, F.Y. Li, Elevated SRPK1 lessens apoptosis in breast cancer cells through RBM4-regulated splicing events, RNA 20 (10) (2014) 1621–1631.
[59] N.S. Chandel, G.R. Budinger, The cellular basis for diverse responses to oxygen, Free Radic. Biol. Med. 42 (2) (2007) 165–174.
[60] A. Hielscher, S. Gerecht, Hypoxia and free radicals: role in tumor progression and the use of engineering-based platforms to address these relationships, Free Radic. Biol. Med. 79 (2015) 281–291.
[61] Y. Perez-Riverol, J. Bai, C. Bandla, D. García-Seisdedos, S. Hewapathirana, S. Kamatchinathan, D.J. Kundu, A. Prakash, A. Frericks-Zipper, M. Eisenacher, M. Walzer, S. Wang, A. Brazma, J.A. Vizcaíno, The PRIDE database resources in 2022: a hub for mass spectrometry-based proteomics evidences, Nucleic Acids Res. 50 (D1) (2022) D543–D552.
[62] A. Lyberopoulou, E. Venieris, I. Mylonis, G. Chachami, I. Pappas, G. Simos, S. Bonanou, E. Georgatsou, MgcRacGAP interacts with HIF-1alpha and regulates its transcriptional activity, Cell. Physiol. Biochem. 20 (6) (2007) 995–1006.